AIP | Review of Scientific Instruments

Optical mapping of fluid density interfaces: Concepts and implementations

X. Zhang, D. Dabiri, and M. Gharib

Citation: Rev. Sci. Instrum. **67**, 1858 (1996); doi: 10.1063/1.1146990
View online: http://dx.doi.org/10.1063/1.1146990
View Table of Contents: http://rsi.aip.org/resource/1/RSINAK/v67/i5
Published by the AIP Publishing LLC.

Optical mapping of fluid density interfaces: Concepts and implementations

X. Zhang,[a] D. Dabiri, and M. Gharib
Center for Quantitative Flow Visualization, California Institute of Technology, 301-46, Pasadena, California 91125

(Received 23 October 1995; accepted for publication 19 February 1996)

Several ideas of color encoding for surface slope measurements are systematically explored and reviewed to develop a new set of fundamental concepts. It is shown that different systems, such as shadowgraphs, Schlieren optics, and our water surface gradient detectors, can also be universally described through the concepts of sun glitter functions, incident light-source encoding, and observer encoding. These concepts provide a more precise way of mathematically formulating and physically interpreting the flow visualization images, thereby providing quantitative results. It is this new system of concepts that uncover the quantitative potential of these optical methods. The measurement abilities of various existing optical systems are thus enhanced from qualitative observation or visualization to the well-defined quantitative measurement. This is a critical step forward. The concepts can also be further extended to measure fluid flows with multiple density layers or flows with continuous density variations. As an example of implementation, the method of measuring a water-surface gradient is extended into a reflective approach of detecting small changes of surface slope at an air–water interface. In this process, fluid surface slopes (surface gradients) are first optically mapped into color space. An array of lenses is used to transform the rays of an optical light source into a series of colored parallel light beams by passing the light through a group of two-dimensional color palettes at the focal planes of the lens array. This system of parallel light beams is used to illuminate a free surface of water. The reflected rays from the free surface are captured by a charge-coupled device color camera located above the surface. The slopes are derived from the color images after the calibration, and surface elevations are obtained by integrating the slopes. This technique is then applied to observe free-surface deformations caused by near-surface turbulence interacting with the free surface. [S0034-6748(96)04405-7]

I. INTRODUCTION

The images obtained from ship wakes have been observed by various remote sensing techniques (e.g., synthetic aperture radar and optical images of sun glitters). The wakes of ships can sometimes extend over hundreds of kilometers. It is still unclear why turbulent ship wakes can last for such a long period of time. Recently motivated by the Navy's goal of understanding free-surface turbulence and its impact on the remote sensing of ship wakes, there has been an increasing interest in the understanding of the nonlinear interaction of vortices and turbulence with a free surface.[1,2] Due to the experimental difficulties in measuring surface deformations, there is still a lack of quantitative information about free-surface deformation and its dynamic evolution. Here, a reflective surface gradient detector, a method integrating digital image processing, optics, and color measurement is presented for measuring two-dimensional (2D) surface deformations.

For nearly a century oceanographers have been attempting to measure the ocean surface shape by observing light reflected or refracted on the sea surface. Most of the early attempts were based on stereo photography.[3]

The probability distribution of water surface slope was successfully obtained in the early 1950s by Cox and Munk[4,5] and others from the average brightness of the sea surface due to incident light from the sun or sky when viewed from above or beneath. Here, the average brightness of the surface is the average number of sun glitters over sufficient time or sufficient surface area. This method does not provide detailed surface structures.

Instead of only measuring the surface slopes of random discrete points or random discrete samples (sun glitters) of a temporally and spatially varying water surface, Cox[6] first developed a single point water surface slope gauge which could continually measure one component of a surface slope in a wind-wave channel. As a result of this study, for the first time, capillary parasitic waves on the forward face of gravity waves were found.

The spatial measurements of short wind waves are not subject to the Doppler effect due to long waves. The first systematic measurement of 2D wave number spectra in wind/wave facilities were conducted by Jähne and Riemer[7] who successfully developed a 2D slope measurement method which uses a video camera system instead of a photocell, and involves a similar light intensity encoding technique.

Zhang and Cox[8] recently developed a color light encoding technique for recording surface gradients (both orthogonal slope components) of an area of water on color films. 2D water surface elevations can then be completely recovered from the recorded gradient data. This technique has been successfully applied to measure short wind waves in a wave tank.[9]

[a]Present address: Scripps Institution of Oceanography, University of California at San Diego, M/S 0230, La Jolla, CA 92093.

 0034-6748/96/67(5)/1858/11/$10.00

In the field of experimental gasdynamics, aerodynamics, and ballistics, the optical methods of shadowgraph and Schlieren have been widely used for visualizing gas density changes. These methods have been developing for centuries. In terms of density changes, a fluid interface between air and water can be viewed as an interface with a density step change. A flow system with a continuous density change can be approximated by many layers of fluid with infinitely small density differences (isopycnal surfaces). There are also fundamental similarities in system configurations between these methods and our quantitative method of measuring a water surface even though they were developed in different fields and with different concepts. As is proposed later in this paper, it is possible to extend the concepts of our method to the color Schlieren to obtain quantitative measurement.

This paper reports a system developed for measuring free-surface deformation due to near-surface turbulence and the fundamental progress in our understanding of different optical systems for fluid measurements. We will first discuss and explore the principle of surface gradient measurements. The intent here is not to provide a simple review but to develop the novel concepts of measuring a fluid surface quantitatively. The different approaches and optical systems, such as surface mapping, shadowgraph, and Schlieren optics, are then addressed under the concepts that are newly developed here: sun glitter function, incident light encoding, and observer encoding. It is shown how these systems can be improved to measure a flow quantitatively by applying the new concepts. In Sec. IV, our implementation of a reflective surface gradient detector is presented in detail. The experimental setup and preliminary results, as applied to measuring free-surface deformations in an experiment of near-surface turbulence, are described in Sec. V.

II. THE OPTICAL PRINCIPLE FOR MEASURING FLUID SURFACE GRADIENTS

In this section, we develop some new concepts and mathematical formulas that can systematically describe our method of measuring water surface slope components. It is shown that the optical geometry of the system is equivalent to the geometry of sun glitters. The function of sun glitter is introduced as the basic element of the observed image. Then, different light encoding concepts are introduced for mapping water surface slopes.

A. Sun glitter functions

Sun glitters are commonly present when one looks on an ocean or river surface illuminated by sunlight. These are images of the sun reflected by a rough sea surface. The same glitter pattern differs substantially when viewed from above and below the sea surface. One of the differences is that the reflected glitter pattern is larger and less luminous than the refracted pattern. This is due to the optical geometry of sun glitters.[10]

For simplicity, let us consider a plane which includes the incident sun rays, the reflecting sun rays from the sea surface, and the observer C (Fig. 1). The following two conditions have to be satisfied for a point on the water surface, O, within the plane to be a sun glitter. Sun glitters will not be seen by this observer if its surface normal vector, **n**, is not in this plane. The other condition that must be satisfied is that the water surface slope component in the plane fit the law of reflection law or refraction relation (Shell's law), respectively, for reflective or refractive viewing.

Thus, knowing the spatial relations of the sun, the observer, and a water surface point of sun glitter, the slope of the water surface can be uniquely determined by the above relations. This is the basic optical principle of measuring water surface slope distributions through sun glitters.

The sun glitters, which are slope-measurable surface points, are often discrete and spaced according to the topography of the water surface. For the special case when the observer is at infinity (Fig. 1), all the observed light rays are parallel. Therefore, all the sun glitters seen by an observer have the same surface slopes, since the light rays coming from the sun are all parallel. Let $f(x,y)$ and $\nabla f(x,y)$ be the water surface and surface gradient. Then the image of sun glitters or sun glitter function, $S(x,y)$, can be defined as

$$S(x,y,\boldsymbol{\theta})=\delta[\nabla f(x,y)-\boldsymbol{\theta}]=\begin{cases}1, & \nabla f(x,y)=\boldsymbol{\theta}\\ 0, & \nabla f(x,y)\neq\boldsymbol{\theta}\end{cases}, \quad (2.1)$$

where $\boldsymbol{\theta}$ is determined by the geometry of the sun and the observer. In the plane of the sun rays and observer, $\theta=\tan[\frac{1}{2}(\theta_s-\theta_o)]$ for the reflective sun glitter pattern, while for the refractive sun glitter image

$$\theta=-\frac{\sin(\theta_s)-n\ \sin(\theta_o)}{\cos(\theta_s)-n\ \cos(\theta_o)}.$$

Here θ_s, θ_o, and α are the angles of the sun, observer (reflection or refraction), and water surface slope also shown in Fig. 1.

An important property of sun glitter functions is that for a single valued surface function $f(x,y)$, sun glitter patterns spatially do not overlap each others, i.e., they are orthogonal to each other:

$$S(x,y,\boldsymbol{\theta}_i)S(x,y,\boldsymbol{\theta}_j)=\delta_{\boldsymbol{\theta}_i,\boldsymbol{\theta}_j}=\begin{cases}S(x,y,\boldsymbol{\theta}_i), & \boldsymbol{\theta}_i=\boldsymbol{\theta}_j\\ 0, & \boldsymbol{\theta}_i\neq\boldsymbol{\theta}_j\end{cases}. \quad (2.2)$$

To measure the slope of more points on a water surface or more slope values, we need more observers or more distinguishable suns (light sources) at different positions (different $\boldsymbol{\theta}$'s). Each sun glitter pattern gives a single value of the surface slope. The techniques of light encoding, to be discussed below, are used to meet these requirements.

B. Incident light encoding through illumination, color, and time

Figure 2 is a schematic drawing of a refractive slope measurement setup of the illumination encoding scheme. An observer, C, is looking vertically down at a point, O, on a water surface. Below the water surface, there is an array of light sources illuminating the surface point, O. For each different surface slope at point O, there is a light ray being refracted toward the observer through the water surface at point O from one and only one of the elements of the light array. As indicated in Fig. 2, our coordinate is chosen with

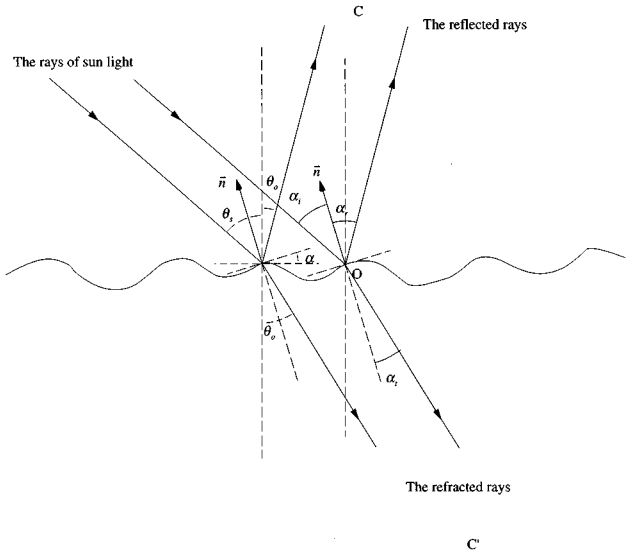

FIG. 1. One-dimensional geometry of sun glitters. It is simplified through moving the observer to infinity.

the z axis pointing vertically upward, the y axis stretching from left to right, and the x axis coming out toward the reader. Let $\nabla f(x,y)=[f_x(x,y),f_y(x,y)]$ be the water surface gradient with two orthogonal components. We encode the light source in such a way that the light intensity varies in the y-axis direction, while remaining constant in the x direction as shown in Fig. 2. The numbers in each of the light cells is chosen to reflect the intensity variations. Thus, the observed light intensity marks the column of the light array, i.e., the y-axis projection (y coordinate) of the light cell position from which the ray originated. Since the position of surface point and the position of the observer are known, the y-direction slope component can therefore be determined from the observed light intensity by

$$f_y(x,y)=\tan(\alpha_{ty}), \quad n\ \sin(\alpha_{ty}-\alpha_{iy})=\sin(\alpha_{ty}), \qquad (2.3)$$

where α_{ty} and α_{iy} are refraction angle and incident angle in $y-z$ plane.

One problem with the setup of Fig. 2 is that the incident angle depends not only on the position of the light cell but also the water elevation. To make the measurement insensitive to the change of surface height, the light source has to be located much farther away and be much bigger (this distance must be much larger than the variations of water surface), as in the sun glitter case. One solution to this problem is to introduce a light encoding lens as shown in Fig. 3.

In this example, a cylindrical lens is placed one focal length above the light array. The light rays from each light cell are refracted through the lens, forming parallel light beams each at different directions depending only on the position of the light cell on the focal plane. This is equivalent to locating each of the light sources at infinity in order to produce a system of parallel beams. Thus, all the light emanating from the water surface points (no matter what the surface elevations or horizontal positions are) having the same light intensity will have the same surface slope y component if the observer is moved to infinity.

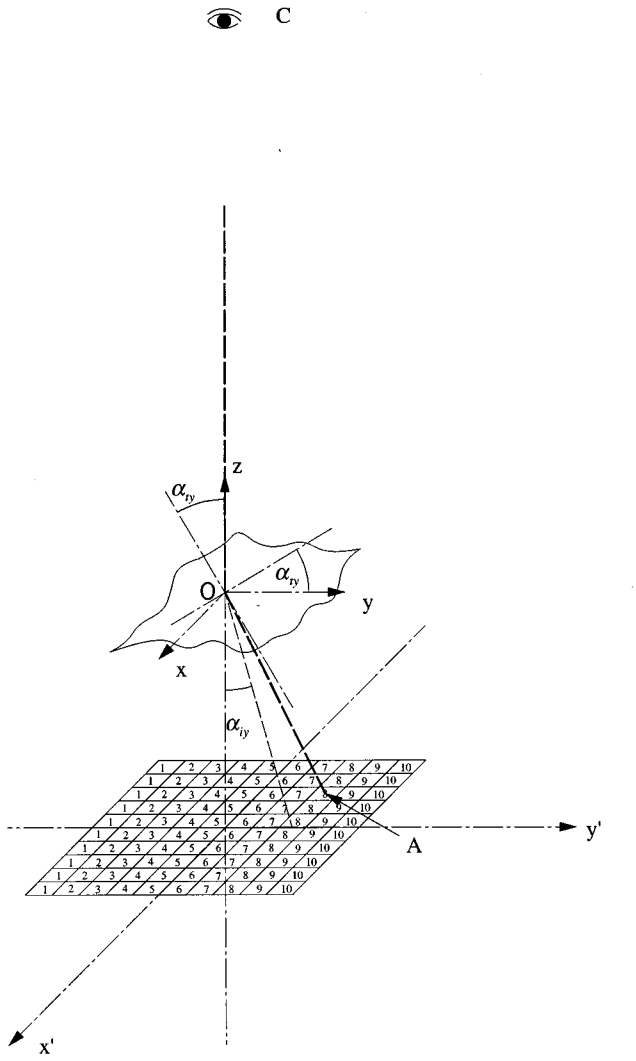

FIG. 2. A schematic drawing of a refractive slope measurement setup of the illumination encoding scheme.

The observer can be moved in closer if we introduce a lens–pinhole system as shown in Fig. 4, where all the light rays refracted through the water surface from below are focused by a lens. Rays of different directions are focused on different spots on the focal plane of the focusing lens. To eliminate all the unnecessary light rays, a pinhole is placed at the center of the focal plane. The light rays that pass the pinhole are then defocused by another defocusing lens.

The resulting images of the y-slope component of the fluid surface can be expressed in terms of the summation of sun glitter patterns weighted by light intensity, I, as follows:

$$\sum_{\theta_y(I)} IS[x,y,\theta_y(I)]=\sum_{\theta_y(I)} I\delta[f_y(x,y)-\theta_y(I)]. \qquad (2.4)$$

It has to be pointed out that if $f_y(x,y)$ is assumed to be a single value function (meaning the surface is not overturned), then images of sun glitters are orthogonal to each other (meaning they are not spatially overlapped). Otherwise, we cannot extract them from the difference in light intensity.

In order to extract both slope components of the water surface slope, colors can be used to encode the incident light.

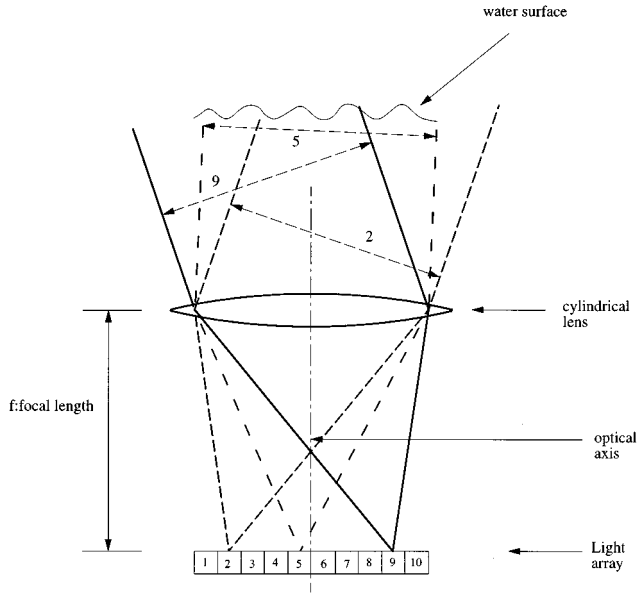

FIG. 3. A lens system for light encoding.

These colors can be represented either by three primaries; red, green, and blue (RGB), or hue, saturation, and intensity (HSI).[9,11] Color space has three degrees of freedom and is more than enough to encode surface gradient space of two degrees of freedom. With a proper choice of color for each light cell in the configuration shown in Fig. 2, the origin of the observed light ray can be traced back through the color of the ray. Therefore, the color of each cell determines each different gradient value. Of course, a spherical lens has to be used instead of the cylindrical lens shown in Fig. 3 in order to encode both surface slope components.[8] Let **c** be a color vector in the color space. The color coded surface gradient image can be formulated as

$$\sum_{\boldsymbol{\theta}(\mathbf{c})} \mathbf{c} S[x,y,\boldsymbol{\theta}(\mathbf{c})] = \sum_{\boldsymbol{\theta}(\mathbf{c})} \mathbf{c}\,\delta[\nabla f(x,y) - \boldsymbol{\theta}(\mathbf{c})]. \tag{2.5}$$

An alternative light encoding method can be used to measure different slopes at different times by flashing each subsequent light cell or pattern of light cells. This method requires that the flash be strong and fast enough to freeze the flow.

C. Observer encoding

The configuration of Fig. 2 can also be reversed so that a light ray can be refracted into water from above. The light cell array is replaced by an optical sensor array. This is a configuration of a system of one sun and many observers. In this setup, each of the optical sensors receives light refracted from one and only one surface slope value. Hence, the ray geometry is found. This is the basic optical principle of the laser scanning slope gauge.[12]

Let us further explore the idea of having different observers. Suppose the sun is directly above the sea surface, which is equivalent to having light emanating from a point source collimated by a lens (Fig. 5). The parallel beam of light is then refracted through the water surface into the water. The direction of light rays is solely dependent on the surface slope. Under the water, there are many observers at different positions. Each of the observers captures the refracted light from one direction, i.e., sun glitters corresponding to a certain surface slope, $S(x,y,\boldsymbol{\theta})$.

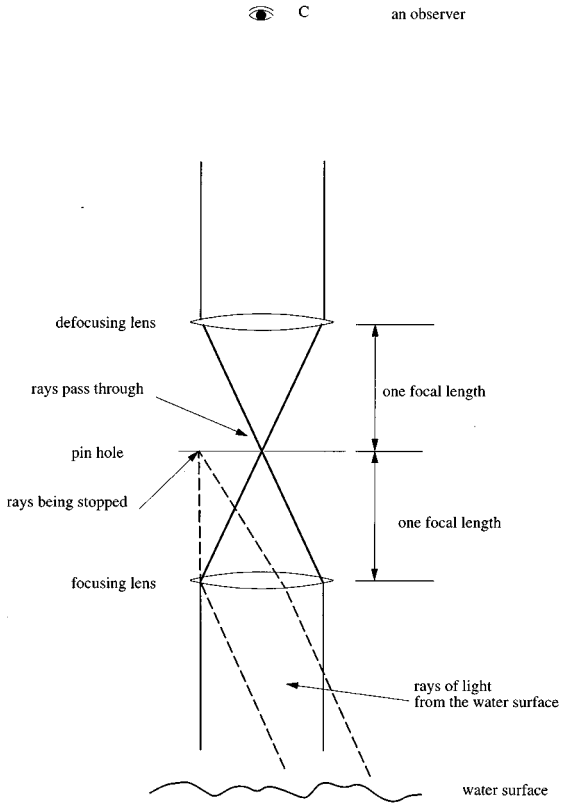

FIG. 4. A lens–pinhole–lens system for filtering of observing light.

The observers can be brought closer to the water surface by a focusing lens. Each observer looks at the water surface through a pinhole located at different positions on the focal plane of the focusing lens. Each pinhole therefore allows only the light rays in a certain direction from the water surface to pass. The pinholes act as a filter to separate each of the sun glitter functions.

Further, color filters of different colors are replaced for the pinholes on the focal plane. The light rays refracted by the different slopes of the water surface are then marked with different colors. Each of those sun glitter colored patterns propagates toward a different direction corresponding to the surface slope. If these color encoded rays are directly projected on an image plane, the sun glitter patterns can overlap each other and they are no longer orthogonal. But with the help of an additional defocusing lens and a light diffusing screen on the imaging plane of the lens, the sun glitter patterns can be shifted back to be orthogonal, and the image of water surface can be recovered from the acquired colors which represent the surface slopes [see Eq. (2.5)]. The proper position of the image plane, H_i, is not arbitrarily chosen. This position is defined as

$$H_i = \frac{f_d}{f_f}(H_w + f_d + f_f), \tag{2.6}$$

where H_i is the distance from the mean water surface to the focusing lens, H_w is the distance from the defocusing lens to the imaging plane, and f_d and f_f are the focal lengths of the defocusing and focusing lenses (Fig. 5). For example, the image on the AA' plane does not allow proper focusing of the light refracted from the surface slopes,

$$\sum_{\boldsymbol{\theta}(\mathbf{c})} \mathbf{c}S\{\mathbf{x}+\mathbf{r}[\boldsymbol{\theta}(\mathbf{c})],\boldsymbol{\theta}(\mathbf{c})\}=\sum_{\boldsymbol{\theta}(\mathbf{c})} \mathbf{c}\delta[\nabla f\{\mathbf{x}+\mathbf{r}[\boldsymbol{\theta}(\mathbf{c})]\}-\boldsymbol{\theta}(\mathbf{c})]. \tag{2.7}$$

The superimposed sun glitter image elements are spatially shifted $\mathbf{r}(\boldsymbol{\theta})$. In this case, the registered sun glitter functions $S\{\mathbf{x}+\mathbf{r}[\boldsymbol{\theta}(\mathbf{c})],\boldsymbol{\theta}(\mathbf{c})\}$ are not orthogonal. From this superimposed sun glitter image, it is very difficult to extract each of the sun glitter images which provides a one to one correspondence to the water surface slope.

In summary, it is shown that the optical geometry can be specified by the function of sun glitters. There are a variety of incident light and observer encoding methods for mapping. For the observer encoding scheme, one must be cautious in choosing the position of the imaging plane.

III. A QUANTITATIVE OPTICAL PRINCIPLE FOR SHADOWGRAPH AND SCHLIEREN METHODS

The configuration of observer encoding of Fig. 5 may look familiar to many readers. In fact, if one were to replace the color filter at the focal plane by a knife edge and use either a point or slit light source, the system becomes a classical Schlieren system. Now, let us discuss an ideal optical color Schlieren system[13] (Fig. 6) in terms of the principles described earlier. It is our intent to show how the concepts developed above can be used to interpret and quantify the shadowgraph and Schlieren optics in a nontraditional manner which further shine light on the nature of these different optical methods which have many similarities.

As is shown in Fig. 6, a plane filter of a certain color pattern is placed on the focal plane of a light encoding lens. The light that passes through a defusing lens, a color pattern filter and a light encoding lens are directionally coded with colors, i.e., the rays of the same propagating direction, to a testing section having the same unique color. The test section contains a transparent fluid (gas) which has a nonuniform optical refractive index caused by various mechanisms (e.g., shock waves). Being refracted by the gas body, the rays of light are then collected by a focusing lens or Schlieren head. On the focal plane of the focusing lens, there is another color pattern filter, or Schlieren stop. The light rays then complete another (post-test section) color encoding, after final propagation through the defocusing lens, before being imaged on to a film or charge-coupled device.

We define the total refraction as the integrated refraction of the light ray through the test section. The total refraction is a vector just like the water surface slope. We can therefore define an imaginary water surface, or an interface of gases or fluids of different densities, $f(x,y)$, which totally refracts the light by the same amount as the gas volume. The combination of color filter and color encoding lens before the test section is equivalent to the incident light encoding system previously described. The configuration of the Schlieren

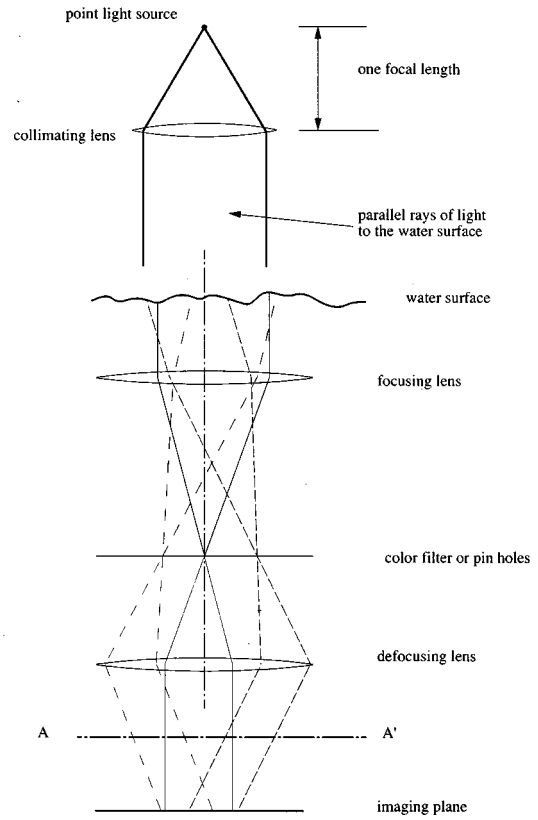

FIG. 5. A schematic drawing of a fluid surface slope detector with observer encoding approach.

head, Schlieren stop, and defocusing lens is the same as an observer encoding setup. Each of the light projections from the test section can be conceptually viewed as sun glitter patterns.

Now, it is possible to construct and define traditional and new optical systems by defining both pre- and post-test section light-encoding filters, and therefore, to interpret the images obtained through these systems by finding the slopes of this equivalent refracting surface. This will then provide a 2D quantitative description of the total volume refraction.

The shadowgraph technique can be described (Fig. 6) by replacing the color filter mask with a pinhole, by replacing the Schlieren stop with a wide open aperture. For the traditional setup, if the open aperture were reduced to a pinhole, the image obtained through the shadowgraph would be equivalent to images obtained from sun glitters $S(x,y,\boldsymbol{\theta})$. As a reminder, the sun glitters indicate a particular direction of the refracted rays. It then follows that if the pinhole is removed, the image obtained through a shadowgraph is the superposition of the images obtained with multiple pinholes. It is important to know where the position of the imaging film is or the plane which the camera is focusing on. Each sun glitter image is registered depending on this position where all elements of sun glitter images are superimposed:

$$\int_{\boldsymbol{\theta}} d\boldsymbol{\theta} S[\mathbf{x}+\mathbf{r}(\boldsymbol{\theta}),\boldsymbol{\theta}]=\int_{\boldsymbol{\theta}} d\boldsymbol{\theta}\delta\{\nabla f[\mathbf{x}+\mathbf{r}(\boldsymbol{\theta})]-\boldsymbol{\theta}\}. \tag{3.1}$$

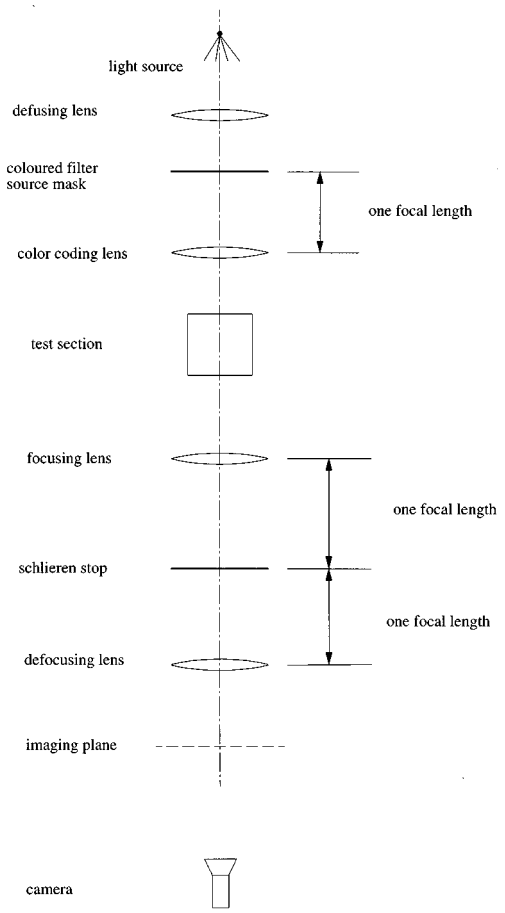

FIG. 6. An ideal optical color Schileren system. In practice, the lenses are often replaced by mirrors.

Here the light absorption of the medium and the change of the refractive index are all ignored. The intensity of a shadowgraph image $I(\mathbf{x})$ is

$$I(\mathbf{x})=N, \tag{3.2}$$

where N is the number of roots of the ray focusing equation in a unit area of image:

$$\nabla f[\mathbf{x}+\mathbf{r}(\boldsymbol{\theta})]=\boldsymbol{\theta} \quad \text{for} \quad \boldsymbol{\theta}\in\{\Theta\}, \tag{3.3}$$

where $\{\Theta\}$ is determined by the size of the aperture. For an ideal geometrical optical system, $\mathbf{r}(\boldsymbol{\theta})\propto\nabla f(\mathbf{x})$. Equation (3.3) can be rewritten as

$$\nabla f[\mathbf{x}+a\nabla f(\mathbf{x})]=\boldsymbol{\theta} \quad \text{for} \quad \boldsymbol{\theta}\in\{\Theta\}. \tag{3.4}$$

The left-hand side of the equation can further be approximated by the Talor's series expansion:

$$\nabla f(\mathbf{x})\cdot[I+a\kappa(\mathbf{x})]=\boldsymbol{\theta}, \tag{3.5}$$

where I and $\kappa(\mathbf{x})$ are the unit and the surface curvature tensor. The larger N is, the more light rays are focused on a point by the curvatures of the equivalent surface. A surface with varying local surface curvatures is acting as a multiple lens with different focal lengths. Light rays are focused or defocused with the focal lens at twice the distance of the center of the local radius. Depending on where the imaging film is, some of the surface curvatures are enhanced while others are not.

The Toepler Schlieren system can be formed by substituting a pinhole for the pretest section filter and a knife edge for the post-test section filter, or vice versa to form what we refer to as a ''reverse Toepler Schlieren system.'' The difference between the traditional and newly suggested reverse systems is whether an observer encoding or an incident light encoding method is applied. Like the shadowgraph, its image is a superimposition of the image projections of total integrated refraction obtained through multiple pinholes of the knife edge. Due to the knife edge, only one-half of the rays of refracted light is imaged resulting in one-half direction with a spatial translation; that is,

$$\int_{\theta_x\geqslant 0}\delta\{f_x[\mathbf{x}+\mathbf{r}(\boldsymbol{\theta})]-\theta_x\}d\theta_x. \tag{3.6}$$

Here $f_x(\mathbf{x})$ is the surface slope vertical to the knife edge direction. For a proper choice of the imaging plane, the spatial translation can be eliminated. Then the resulting image is

$$U(f_x(\mathbf{x})-0)=\begin{cases}1, & f_x(\mathbf{x})\geqslant 0\\ 0, & f_x(\mathbf{x})<0\end{cases}. \tag{3.7}$$

Here $U(x)$ is the step function. The case of finite size of light source can be discussed as the integral image from multiple point light sources. A point light source off the optical axis on the focal plane of the color encoding lens generates a parallel beam of rays with an angle toward the test section. Since the position of the knife edge is fixed, the refracted image is the superimposition of sun glitter function with surface slopes greater than a certain value, a, depending on the angle of incident light; hence, the position of the light source. Without spatial translation, we have

$$U(f_x(\mathbf{x})-a)=\begin{cases}1, & f_x(\mathbf{x})\geqslant a\\ 0, & f_x(\mathbf{x})<a\end{cases}. \tag{3.8}$$

Assuming the size of the light source in the vertical direction of the knife edge is l, the focal length of the coding lens is f, and the corresponding maximum and minimum light incident angles are $l/2f$ and $-l/2f$, then the Schlieren image is

$$\int_{-l/2f}^{l/2f}U[f_x(\mathbf{x})-a]da\propto[f_x(\mathbf{x})-l/2f] \quad \text{for} \quad -l/2f\leqslant f_x(\mathbf{x})\leqslant l/2f. \tag{3.9}$$

That is, the intensity of the Schlieren image is proportional to the surface slope of the surface. This is a case where both incident light encoding and observer encoding are used together. Again, in order to extract the quantitative information from the Schlieren image, the position of the image plane has to be right to avoid the spatial translation of each of the sun glitter elementary images.

The superimposed image is not sensitive to the position of the film for the reverse Schlieren system proposed here, which is an advantage over the traditional method with a Schlieren stop unless the shifting is desired. The spatial translations of each refraction glitter image may reflect or

may tend to obscure the 2D features of the superimposed image. It does not necessarily always give the first derivative of a flow density field. This has been generally overlooked in early studies.

Dark field Schlieren systems select a pinhole for the pretest section filter and a ring-shaped filter for the post-test section filter. The positions of the pinhole and the ring-shaped filter can be switched to produce what we refer to as the reverse dark field Schlieren system. Its image is a superimposition of images of the total integrated refraction obtained through multiple pinholes of the ring. However, due to the circular filter, only the magnitude of the refraction is obtained without regard for its direction. For the zero refraction, the light that passes through the testing section is blocked out due to the ring filter. This is why it is called a dark field system. The expression for the image of a dark field system is

$$U[f_r(\mathbf{x})-r_1]U[r_2-f_r(\mathbf{x})]=\begin{cases}1, & r_2\leqslant f_r(\mathbf{x})\leqslant r_1\\ 0, & \text{else}\end{cases}, \tag{3.10}$$

where r_1 and r_2 are defined by the size of the ring and focal length of the lens and $f_r(\mathbf{x})$ is the slope in radial direction.

Classic color Schlieren is formed by placing a pinhole for the incident light encoding before the test section and a 2D color pattern screen for the color filter after the test section. The positions of the pinhole and the 2D color pattern can be reversed to produce a dissectional color Schlieren.[13–15] The colors of the observed image map the vector of the total integrated refraction. It is claimed that dissectional color Schlieren is more sensitive than the classic color Schlieren. This is now clearly evident since it avoids spatial translations in superimposing. The study by Kleine and Grönig[13] shows that the dissectional color system can be made equivalent or even superior to traditional black-and-white techniques. The classic color Schlieren can also achieve the same sensitivity if the position of the film is chosen right, but often is not. The dissectional color Schlieren has, in fact, the same optical setup as our surface gradient detector which is capable of providing 2D quantitative information of total refraction.

A more generalized color Schlieren system is a system adapting one or both color pattern filters instead of black-and-white filters or stops only. One must be extremely careful when interpreting the acquired image with both pre- and postcolor filters, or both light encoding and observer encoding. For most cases, two color filters can be redundant and can be replaced by one color and one white filter.

The concepts of sun glitter function (or refraction projection), incident light coding, and observer coding developed here are essential. It functionally unifies the different optical techniques of similar configurations and provides a clear interpretation of what contents are represented by the images of different optical systems, or how many sun glitter images of the equivalent total refraction surface are superimposed. The quantified mathematics of Schlieren images of different systems can thus be formulated based on these new concepts.

The above analysis presents clear concepts of somewhat vague terminology, such as the sensitivity of Schlieren images. It is actually a question of what ranges of a total integrated refraction vector one wishes to resolve through different encoding schemes and how these element images of sun glitters are shifted and superimposed together. In the early studies, attempts to enhance the sensitivity of Schlieren images involved reducing the size of the Schlieren stop, slit, or filter segments. The importance of the chosen position of the image plane has been widely overlooked to date. To extract the quantitative 2D information of total refraction by a fluid body rather than qualitative visualization only, it is important to keep the registration of sun glitter images as small as possible.

It should be made clear that the purpose here is not to claim one system is superior to other systems. By combining advantages of different systems and theories, the full potential of optical techniques can be more efficiently used for different applications. Many reviews have been written on Schlieren techniques over the years[15,16] which cover the different aspects of the subject.

IV. A REFLECTIVE APPROACH OF 2D SURFACE GRADIENT MEASUREMENT

The concepts of water surface gradient mapping are discussed above. Here, as an example of implementation, a reflective 2D surface gradient detector is presented. This method images the water surface through the reflected rather than refracted light and employs the light color encoding scheme. Because of the high surface slope sensitivity of this setup, it fits well for measuring free-surface deformation due to near-surface turbulence.

A. Geometry of reflective approach

Suppose one observes reflected light on a point, O, on a water surface at a fixed angle of γ from vertical as shown in Fig. 7(a). The direction of the incoming light ray, β, which is reflected into the angle γ, only depends on the water surface slope α according to the law of light reflection. For example, for a zero water surface slope, as indicated in Fig. 7(a) by red lines, the incoming angle of the red light ray, β_0, is equal to γ. However, as shown in Fig. 7(a) by blue lines, when the water surface has a slope angle of α, the incoming angle of the light ray, β_1, is equal to $\gamma+2\alpha$. For every 1° surface slope change, there is a 2° change of the incoming ray angle,

$$\beta_1-\beta_0=2\alpha. \tag{4.1}$$

The larger the change of the ray angles, the easier it is for one to detect these changes; hence, the higher sensitivity. The same principle applies to observing refracted light through a water surface as shown in Fig. 7(b). But, for every 1° change of surface slope angle, there is only about 1/4° of change in the incoming angle [Eq. (2.3)], where the observational angle, γ, is set to zero. The reflection geometry here is much more sensitive to the surface slope change than the refraction geometry. However, the range of slopes that can be measured is smaller for the reflective scheme than for the refractive scheme. Therefore, the scheme chosen should depend on application.

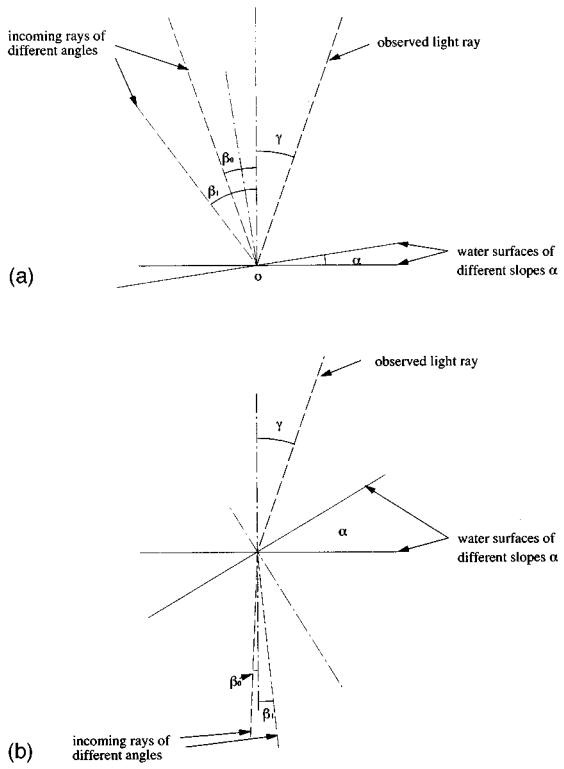

FIG. 7. Optical geometry of slope detectors: (a) a reflective approach; (b) a refractive approach.

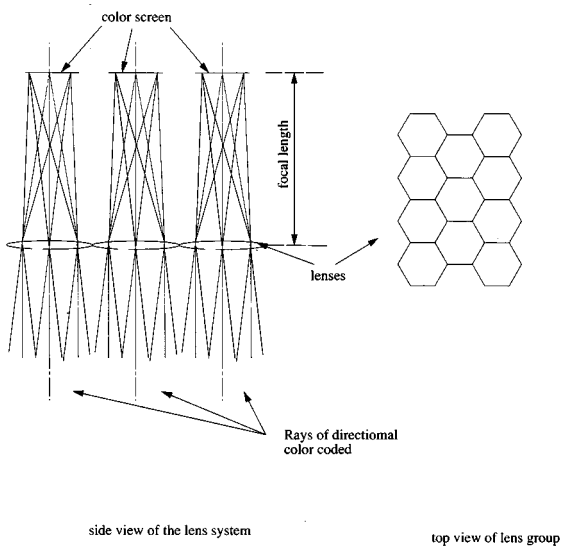

FIG. 8. The synthentic lens system.

B. Incident light coding system

The incoming light rays can be color coded with a simple collimating lens system. Here, a group of hexagonal-shaped lenses identical in dimension and focal length form a plane acting as a single larger lens (Fig. 8). The purpose of using a group of lenses instead of one lens is to reduce the dimensions involved with the optical system, or to reduce the effective $f/\#$ (effective focal length/effective lens diameter), given the same dimensions of the system. In principle, one can always consider the lens group as a single lens.

For a specified maximum angle of the slope, $\alpha_{\max}$, which the system can measure, the maximum angle of the encoded light rays, $\beta_{\max}$, must be twice as large. Let f be the focal length of the collimating lens, and R_s be the radius of the color coding screen. Further assume that R_s is the same size as the lens, R, then

$$\beta_{\max}=\tan^{-1}\left(\frac{R_s}{f}\right)\leqslant\tan^{-1}\left(\frac{R}{f}\right)=\tan^{-1}\left(\frac{1}{2f\#}\right), \tag{4.2}$$

where R_s can be smaller than R of the lens, but then the $f/\#$ has to be even lower. The higher the $f/\#$ is, the better the performance and cheaper the lens are. The size of the lens has to be larger than the area of measurement. For a $\beta_{\max}$ of 8°, the highest $f/\#$ is 3.7. For a 30-cm-diam lens, a 107 cm focal length is needed, making the size of the light encoding system very big. Further, a good quality, low $f/\#$, and large size lens is extremely expensive. We currently use fresnel lenses, making it even more imperative to keep the $f/\#$ as high as possible for performance reasons. A solution to reduce the focal length while keeping a high $f/\#$ per lens is to use a lens array. The $f/\#$ of each lens element determines the optical quality, and the combined size of lens array decides the size of the measurement area.

The area of the water surface that can be measured by our method is dependent on the size of the collimating lens and the distance from the lens to the water surface. To resolve all the measurable slopes, the measurement area of the water surface has to be covered by color-coded light rays in all directions. Let $L_{\max}$ be the horizontal size of the water surface area to be measured, MD the size of the lens array, and H be the vertical distance from the center of the lens to the water surface. Then,

$$L_{\max}\approx MD-2H\ \tan(\beta_{\max}),$$

$$\begin{aligned}L_{\max}=&MD/\cos(\gamma)-\{H[\tan(\beta_{\max}+\gamma)-\tan(\gamma-\beta_{\max})]\\&+\sin(\gamma)MD[\tan(\gamma)-\tan(\gamma-\beta_{\max})/2\\&-\tan(\beta_{\max}+\gamma)/2]\}\\\rightarrow&MD-2H\ \tan(\beta_{\max}),\quad \gamma\rightarrow 0,\beta_{\max}\rightarrow 0.\end{aligned} \tag{4.3}$$

C. Color screen and light source

The color pattern of the screen used here is the same as the HSI scheme of Zhang and Cox[9] but instead of a circular shape, we adapted the hexagon shape [Fig. 9(a)] to correspond to the hexagonal lenses. Each lens has its own separate color pattern, and all the color patterns are identical. In this 2D color configuration, the hue of colors gives the azimuth of the water surface gradient, and the saturation of the colors nearly specifies the magnitude of the surface gradient. The surface color images are captured in a primitive RGB base, and the corresponding hue, saturation, and intensity (HSI) which are used for recovering the surface gradient can then be calculated from the RGB signals. The advantages of using the HSI scheme was discussed earlier.[2] The separated RGB

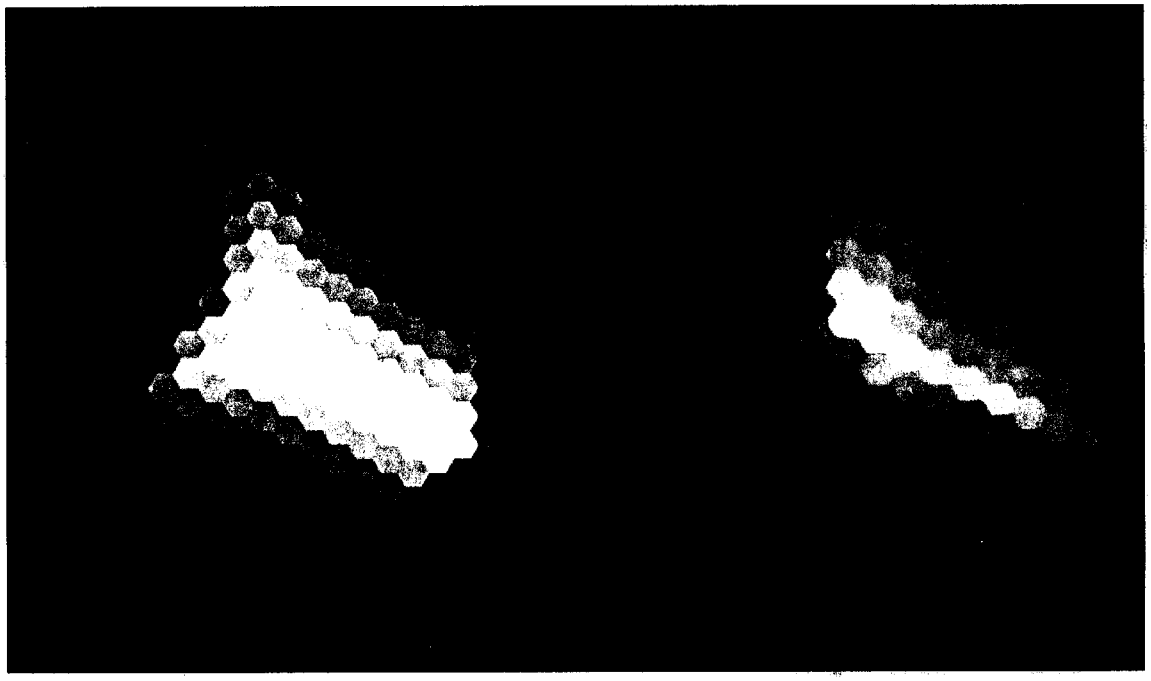

FIG. 9. (a) The color pattern used for color coding the free-surface slopes. (b) The calibration image taken by a RGB video camera.

signals from the camera can be digitized directly to a computer via a frame grabber or recorded separately on three video disks.

The light reflection on the water surface is much weaker than the light transmission. The ratio of reflection and refraction index is about 1/48. We use three strobe lights strobing simultaneously as the light source. The strobe lights provide a strong light pulse for 10 μs, thereby freezing the surface. This pulse is timed at the beginning of each frame of the video camera to yield full frame spatial resolution.

D. Observing system

For incident light encoding only, the focusing lens, the pinhole, and defocusing lens for observer encoding can be omitted by moving the camera far away. How far away the camera should be placed is decided by the slope resolution of the system. The designed slope resolution is dependent on the size of each color cell within the color pattern. Let the size of each color element be ΔCL, and the slope sensitivity be $\Delta\alpha$. Then,

$$\Delta\alpha \leqslant \tan^{-1}(\Delta CL/f)/2. \tag{4.4}$$

Let D be the diameter of each lens element in the color coding lens array, and TC be the distance from the camera to the water surface. The camera view angle is approximately:

$$\tan^{-1}\left(\frac{D}{TL}\right) \approx \frac{D}{TL}. \tag{4.5}$$

The viewing angle of the camera has to be less than twice the slope sensitivity. Combining Eqs. (4.5) and (4.4) and using the small angle approximation:

$$TL \geqslant f\,\frac{D}{\Delta CL}. \tag{4.6}$$

Another advantage of using a lens array instead of a single collimating lens is the reduction of the distance of the camera to the water surface which increases the camera light exposure.

E. Data processing

In order to capture the evolution of near-free-surface vortices and turbulence, a three-chip RGB color CCD camera is used to record real-time image sequences of the surface gradient. Although video images have lower spatial resolution than photographic film, a good color balance of the video images can be achieved electronically rather than chemically by processing photographic film. There are high resolution color CCD cameras available. The real time digital recording at very high spatial resolution is still extremely expensive.

The color water surface images captured by the camera are digitized into a computer for analysis. The data analysis method has been described in detail.[9] Through the use of the calibration images, colors are translated into gradients of the water surface. The reconstruction of the surface elevation is done in Fourier space.[17,18]

V. EXPERIMENTAL SETUP AND SOME PRELIMINARY RESULTS

The experimental setup for studying the interaction of turbulence with the free surface using this reflective gradient detector is shown in Fig. 10. In a cubic water tank of about 40 cm of each dimension, the small scale homogeneous turbulence is initially generated by dropping a grid. The grid is a perforated plate ($\sim$60% open area) with 0.8 cm hole diameters. The water is cleared with a special water filtering system to minimize the surfactant effect. Also, the newly

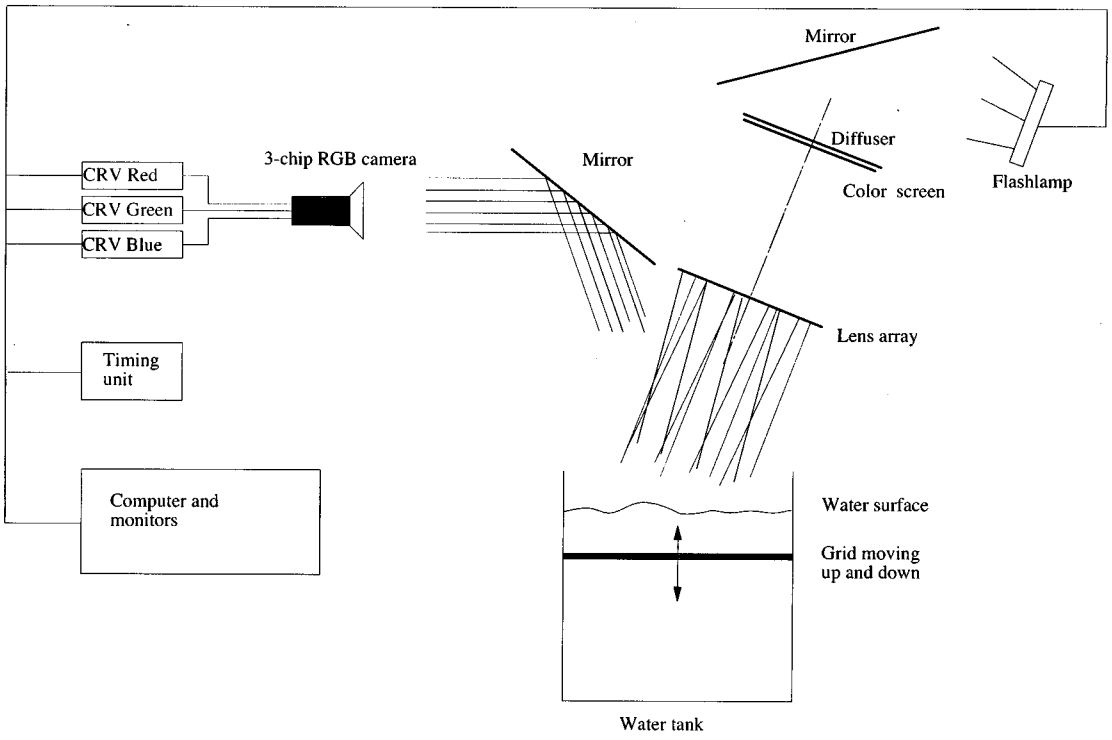

FIG. 10. The experimental setup for measuring the free-surface deformations due to near-surface turbulence.

formed surface film is drawn out before each run of our experiment. The light from the flash lamps are reflected onto the color screen through a light diffuser by a mirror. The light rays, now color coded by the combination of the color screen and the lens array, propagate to the water surface. The color screen and lens array are chosen and setup to respond to surface slopes from $-4°$ to $4°$. The surfaces of the turbulence-generating grid in the water and the bottom of the water tank are sand blasted and made of black plastic to eliminate the light reflections from anything other than from the water surface. A three-chip CCD RGB camera records in real time the water surface color images from 6 m away through a mirror. The acquisition is done in real time, thereby allowing for analysis of time-evolving flows. The three primitive RGB signals of the captured images are separately recorded on three video laser disk recorders so that the full spatial and chroma resolution of the color signal are preserved. After acquisition, recorded images are read back to a computer to analyze the data in order to extract the surface information.

The reflective gradient detector is carefully calibrated to reduce the measurement bias due to the imperfection of the apparatus. A spherical mirror is used as the curved calibration surface. The color image of the spherical concave surface of the mirror recorded by the camera is shown in Fig. 9(b). The hue of color image changes with the azimuth of the surface slope and the saturation of the color changes nearly according to the magnitude of the surface slopes. The image analysis and calibration schemes have been described in some detail.[2]

Figures 11(a) and 12(a) show two sequential raw images acquired in our experiment with a 0.1 s time interval. It

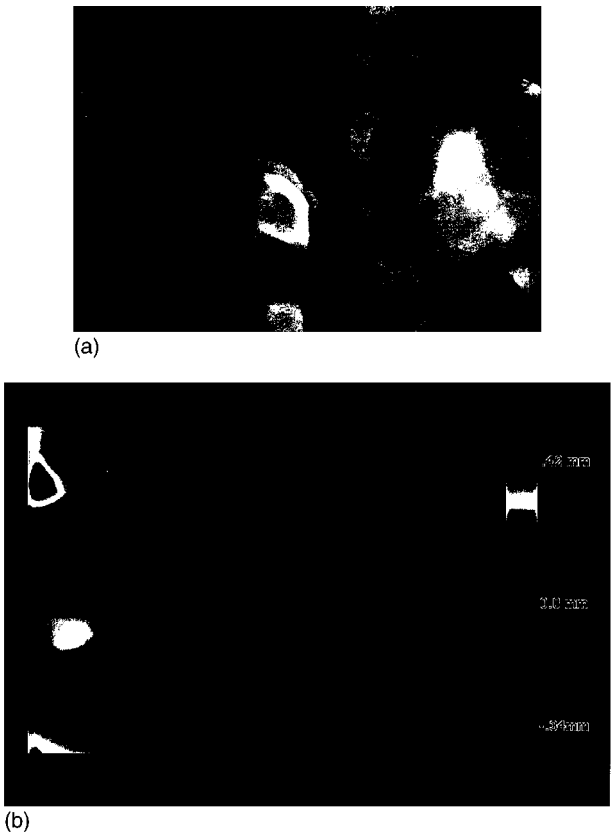

FIG. 11. A free-surface picture was captured 10 s after starting to move the grid from the surface to the bottom of the tank. The free surface is deformated by the turbulence generated within the volume of the fluid. The image covers an area of 22 cm by 15 cm: (a) surface gradient image; (b) surface elevation image extracted from the gradient image.

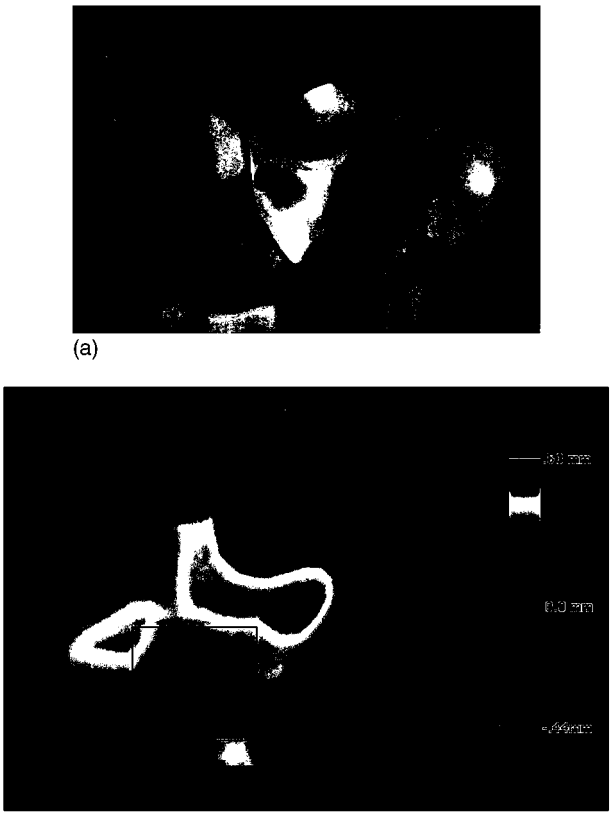

FIG. 12. A picture of free surface was captured 0.1 s after Fig. 11. All specifications are identical to those given for Fig. 11. Also, circular color patterns similar to the color pattern shown in Fig. 9 are seen showing the evolution of the vortex connecting with the free surface as compared with Fig. 11: (a) surface gradient image; (b) surface elevation image extracted from the gradient image.

should be emphasized that the raw images are not pseudocolored or processed in any way. The images cover an area of the water surface about 22 cm×15 cm and are captured 10 s after starting to move the grid from the surface to the bottom of the tank. The dark curved lines in the images are due to connecting edges of lens array where the light rays cannot pass through and reach the water surface. These dark lines are the edges of the lenses within the lens array, and can be filtered out through digital image processing. For the surface structure of a dip of a vortex connected to the free surface, the azimuth of the water surface slope changes around the center of a vortex. A surface color image with this kind of dip structure is expected to have a change in the hue of colors around the vortex center similar to the calibration image of Fig. 9(b), that is, red on the bottom portion, green on the upper right portion, and blue on the upper left-hand portion of the image. As we can see from Fig. 11(a), there is a clear circular structure, 7 cm in diameter, in the bottom left-hand portion image with red at the bottom, green on the upper right-, and blue on the upper left-hand side. There are also a few less enhanced similar color patterns in the background of Fig. 11(a). Similar circular color patterns can also be found in Fig. 12(a).

Figures 11(b) and 12(b) are corresponding pseudocolored surface elevation images calculated from the directly measured image data of Figs. 11(a) and 12(a). The surface elevations from the mean water surface are less than a half a millimeter. A vortexlike structure is marked in the succeeding images Fig. 11(b) and Fig. 12(b) which are 0.1 s apart.

ACKNOWLEDGMENTS

This work has been supported by the Office of Naval Research Fluid Dynamics Program (ONR-URI, Grant No. N00014-92-J-1610). X.Z. thanks Professor C. S. Cox for many suggestions and discussions.

[1] A. T. Sarpkaya, AIAA 92-0057, 30th Aerospace Sciences Meeting, Reno, NV, 6-9 January, 1992.
[2] M. Gharib, D. Dabiri, and X. Zhang, 1994 ASME Fluids Engineering Division Summer Meeting, Lake Tahoe, NV, 19–23 June, 1994 (unpublished).
[3] B. Jähne, J. Klinke, and S. Waas, J. Opt. Soc. Am. A **11**, 2197 (1994).
[4] C. S. Cox and W. Munk, J. Marine Res. **13**, 198 (1954).
[5] C. S. Cox and W. Munk, J. Opt. Soc. Am. **44**, 838 (1954).
[6] C. S. Cox, J. Marine Res. **16**, 199 (1958).
[7] B. Jähne and K. S. Riemer, J. Geophys. Res. **95**, 11531 (1990).
[8] X. Zhang and C. S. Cox, EOS Trans. Am Geophys. Union **72**, 276 (1991).
[9] X. Zhang and C. S. Cox, Exp. Fluids **17**, 225 (1994).
[10] C. S. Cox and W. Munk, J. Marine Res. **14**, 63 (1955).
[11] D. Dabiri and Gharib, Expt. Fluids **11**, 77 (1992).
[12] S. R. Long and N. E. Huang, J. Fluid Mech. **77**, 209 (1976).
[13] H. Kleine and Grönig, Shock Waves **1**, 51 (1991).
[14] P. H. Cords, SPIE J. **6**, 85 (1968).
[15] G. S. Settles, in *Flow Visualization*, edited by W. Merzkirch (Hemisphere, New York, 1982), Vol. II, p. 749.
[16] H. Schardin, Ergeb. der Exakt. Naturwiss. **20**, 303 (1942) (trans. NASA TIF-12731, 1970).
[17] X. Zhang, Ph.D. dissertation, University of California, San Diego, 1993.
[18] X. Zhang, Expt. Fluids (to be published).